Chapter 1

Introduction

This thesis describes the formulation of a mathematical model describing the signal generation process in both the reflectance and magneto-optic, Type 1 and Type 2, scanning optical microscopes. The model has been implemented in computer code and allows the analysis and investigation of a variety of imaging techniques commonly used in the field of scanning optical microscopy. Two separate signal generation techniques, the 'direct calculation' and 'transfer function' approaches are presented and their applications studied.

1.1 The scanning optical microscope

The conventional microscope is a versatile instrument commonly used in many scientific fields for producing high magnification images of objects. In the conventional microscope an area of the object is illuminated by a spot of light and is simultaneously imaged by the eye, or viewed directly on a screen.

An alternative microscope arrangement, the scanning optical microscope (SOM) was first illustrated by Roberts and Young in the 1950s. Their 'flying spot' microscope employed a cathode ray tube to generate a scanning spot of light which was then transmitted through the optics of the conventional microscope in reverse to produce a scanning spot on the surface of the object. The light transmitted through the object was then detected using a photocell and the electrical signal was displayed on a TV screen [2]. In 1969 the first scanning laser microscope (SLM) was demonstrated by Davidovits and Egger [3]. In their system a 5mW HeNe laser light source was scanned across the surface of the object in a raster like fashion using a *x-y-z* scanning objective. The introduction of the SLM lead to the implementation of a variety of further imaging techniques. A prime example is the confocal scanning microscope

which is often used in biological spheres and offers important depth discrimination properties and improved resolution over the conventional microscope.

The scanning laser microscope offers many advantages over the conventional microscope. These include :

- Improved resolution using the confocal scanning microscope, 1.4 x that of the conventional microscope.
- No chromatic aberrations since the laser is monochromatic.
- High numerical apertures can be used at all magnifications.
- Electronic processing and optical resolution improvement techniques may be implemented with greater ease than is possible with the conventional microscope.
- Image brightness and contrast is controlled electronically rather than by the optics.
- Numerous imaging modes possible.
-

Figure 1.1 illustrates the optical layouts of the common forms of scanning optical microscope.

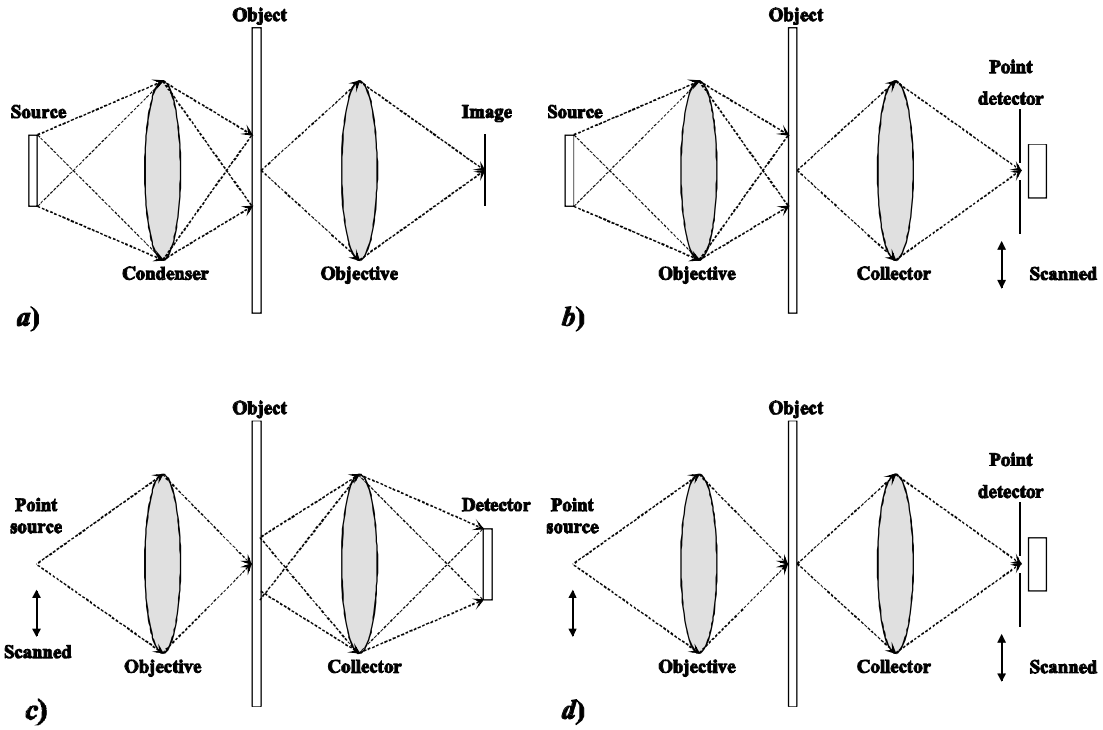

Figure 1.1 : *Scanning optical microscope arrangements : a) the conventional microscope, b) the Type 1a scanning microscope, c) the Type 1b scanning microscope, d) the Type 2, or confocal, scanning microscope.*

Figure 1.1 (*a*) illustrates the optical arrangement of the conventional microscope. In this configuration the object is illuminated by a patch of light from an extended source through a condenser lens. The object is then imaged through an objective lens and viewed using a eyepiece. The resolution of the conventional microscope is determined primarily by the quality of the objective lens.

Figure 1.1 (*b*) illustrates the optical arrangement of a scanning microscope based around the arrangement of the conventional microscope; the Type 1*a* scanning microscope. Here, a point detector is scanned through the image plane, such that it detects a small region of the image at any instance in time. The image is constructed point by point and displayed on a colour monitor.

Figure 1.1 (*c*) illustrates the optical arrangement of the Type 1*b* scanning microscope. Here, a point source is focused onto the object through an objective lens. The detector measures the total amount of light that is transmitted through, or reflected from, the object. The image is constructed by scanning the point source across the object, thus constructing an image point by point. Alternatively, the object is scanned with respect to the stationary focused spot. The Type 1*b* configuration is commonly referred to simply as the Type 1 scanning microscope.

Figure 1.1 (*d*) illustrates the optical arrangement of the Type 2, or confocal, scanning microscope. Here, a point source is again focused onto the object through an objective lens. After interaction with the object the light passes to a point detector. An image is constructed by scanning the point source and point detector in synchronism across the object. The term *confocal* is used to indicate that both the objective and collector lenses are focused on the same point on the object [4].

Many authors have illustrated the imaging similarities between the conventional and the Type 1 scanning microscopes [4,5,6]. It can be shown that the imaging characteristics of the two configurations are similar providing the properties of the objective lenses are identical and that the collector lens of the Type 1 scanning microscope and the condenser lens of the conventional microscope have the same pupil characteristics. This relationship is true providing the effective source in the

scanning microscope is infinitesimal, i.e. the incident illumination is coherent, as with a laser. The confocal configuration, however, offers very different imaging characteristics compared with the conventional microscope, and has improved resolution characteristics over the Type 1 configuration. In the confocal system both the objective and collector lenses determine the imaging characteristics of the optical system. The confocal configuration has important resolution enhancement and depth discrimination properties.

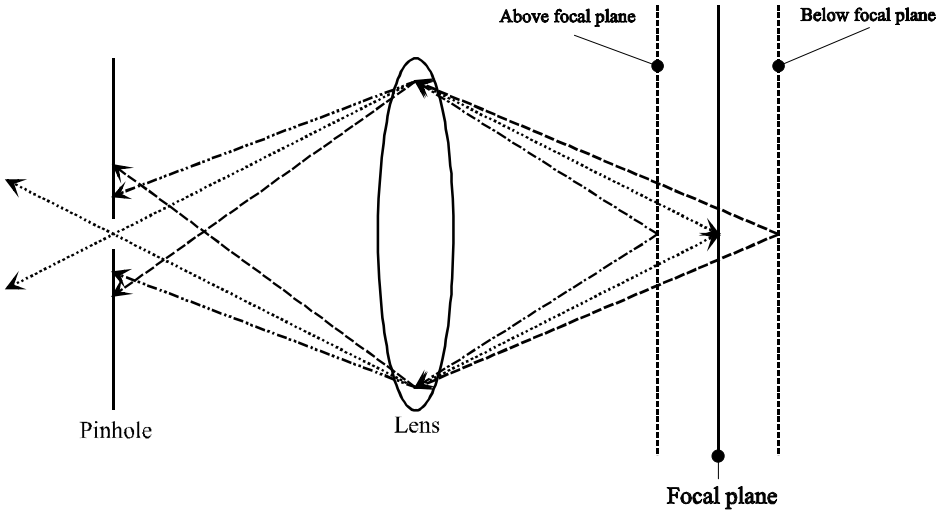

Figure 1.2 : *The depth discrimination properties of the confocal scanning microscope.*

The depth discrimination effect is used to great advantage in biological applications where 3-D images of transparent or semi-transparent objects are generated. Its origins are illustrated in Fig. 1.2 where it can be seen that only light originating from within the focal plane of the lens is brought to focus in the plane of the pinhole and propagates through the pinhole aperture to reach the photo-detector. Light from above the focal plane is brought to focus after the plane of the pinhole, hence, very little light propagates through the pinhole aperture towards the detector. Light from below the focal plane is brought to focus before the plane of the pinhole, and again very little light propagates through the pinhole aperture towards the detector. Hence, the signal from the detector in the confocal configuration is extremely sensitive to the degree of focus.

Due to the versatility of the scanning optical microscope it has an exceptionally wide range of applications and may be used to investigate the properties of objects using a variety of imaging and contrast techniques. A particular use of the scanning microscope is in the field of magneto-optics [8,9,10]. It has been shown that by the modification of the optics of the ordinary scanning microscope and by using a coherent polarised source, such as a laser, the scanning microscope may be used to image magneto-optic (MO) contrast. Such an instrument has been shown to have particular advantages in the investigation of the properties of a range of thin films and devices such as magneto-optic storage materials, magneto-resistive sensors and magnetic multi-layers [11,12,13,14,15]. The study of MO techniques forms a major part of the work of this thesis.

1.2 The magneto-optic effects

The magneto-optic effects are characterised by a change in the state of linearly polarised light upon reflection from, or transmission through, a magnetic surface. The first interaction between light and magnetic materials was recorded by Michael Faraday in 1845. Faraday observed that linearly polarised light was rotated upon transmission through lead glass in a magnetic field [16], as illustrated in Fig. 1.3 (*a*) . Later in 1897, John Kerr discovered that the plane of polarisation of linearly polarised light was rotated upon reflected from the poles of an magnet, the magnitude of the rotation being proportional to the net magnetisation [17].

The form of the magneto-optic interaction depends upon the direction of polarisation with respect to the plane of incidence and the direction of magnetisation. When the incident light is linearly polarised in a direction parallel, or perpendicular, to the plane of incidence, then the *polar Kerr* and *longitudinal Kerr* effects produce a small, magnetisation sensitive, rotation of polarisation. The polar Kerr signal is maximised when the polarised light is normal to the magnetic surface, as illustrated in Fig. 1.3 (*d*). The longitudinal Kerr signal is maximised when the polarised light is incident at an angle of 60° to the normal of the magnetic surface, as illustrated in Fig. 1.3 (*c*). A further magneto-optic effect, the *transverse Kerr effect*, is characterised by the

attenuation of the magnitude of linearly polarised light upon reflection from a magnetic surface, and is illustrated in Fig. 1.3 (*d*) [18,19,20,21].

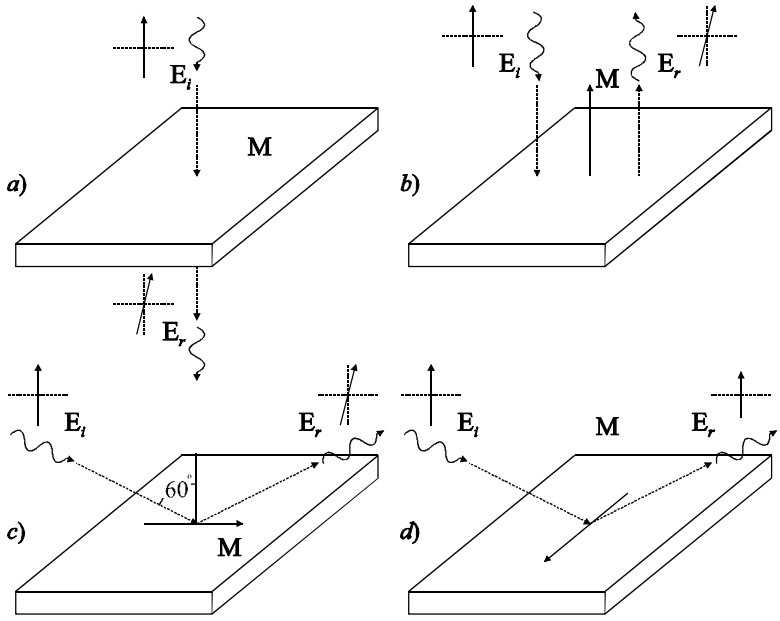

Figure 1.3 : *The magneto-optic effects : a) the Faraday effect, b) the polar Kerr effect, c) the longitudinal Kerr effect and d) the transverse Kerr effect.*

The magneto-optics effects can be described in terms of quantum mechanical interactions between light and the effective magnetic field due to the spin-orbit interaction of atomic atoms [22]. However, such a description is beyond the scope of this thesis. Instead, a phenomenological approach is used for which it is useful to first grasp the properties of the polarised optical field.

1.2.1 The polarised optical field

A monochromatic, uniform plane wave propagating in free space, or an isotropic medium, can be expressed in the form

$$\begin{aligned} y(x,y,z,t) &= \left(y_x\hat{x} + y_y\hat{y}\right)\exp\left(j(kz-wt)\right) \\ &= \left(y_{ox}\exp\left(jf_x\right)\hat{x} + jy_{oy}\exp\left(jf_y\right)\hat{y}\right)\exp\left(j(kz-wt)\right) \end{aligned} \tag{1.1}$$

where y_x and y_y are orthogonal field components and it is assumed the wave is propagating in the *z* direction in a Cartesian co-ordinate system, where $\hat{x}$ and $\hat{y}$ are

unit vectors. Equation (1.1) describes the propagating electric field **E**, also referred to as the optical field. The polarisation state of the propagating optical field is determined by the relative amplitudes of y_{ox} and y_{oy}, and their relative phase difference, $(f_x - f_y)$. Generally eq. (1.1) represents an electric field vector, the tip of which describes an ellipse in the (*x*, *y*) plane, rotating through one complete cycle as the wave propagates one wavelength in the *z* direction.

Linear polarisation

If the phase difference between y_x and y_y is zero or $\pm 2np$, where *n* is an integer, the wave is said to be linearly polarised since the optical field oscillates along a line which is at an angle q with the x - axis, where q is given by

$$q = \arctan\left(\pm\frac{y_{ox}}{y_{oy}}\right) \tag{1.2}$$

as illustrated in Fig. 1.4.

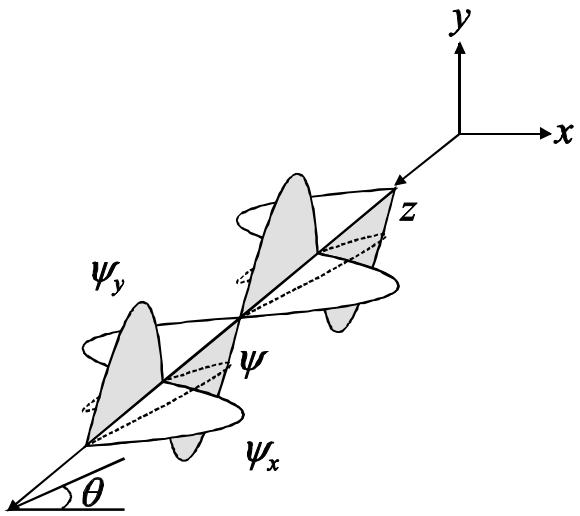

Figure 1.4 : *Linearly polarised optical field.*

Circular polarisation

If the magnitude of y_x and y_y is equal, i.e. $y_{ox} = y_{oy} = y_o$, and the phase difference, $(f_x - f_y)$, is $-p/2 \pm 2np$, such that

$$y(x,y,z,t) = y_o(\hat{x} \pm j\hat{y})\exp(j(kz - wt)) \tag{1.3}$$

then the optical field is of constant scalar amplitude at any particular value of *z*, and the tip of the vector describes a circle in the (*x*, *y*) plane. The plus / minus sign indicates the direction of rotation. Plus (+) indicates anticlockwise rotation, looking back at the source, and is referred to as left circularly polarised (LCP), and negative (−) indicates clockwise rotation and is referred to as right circularly polarised (RCP). Figure 1.5 illustrates the LCP optical field.

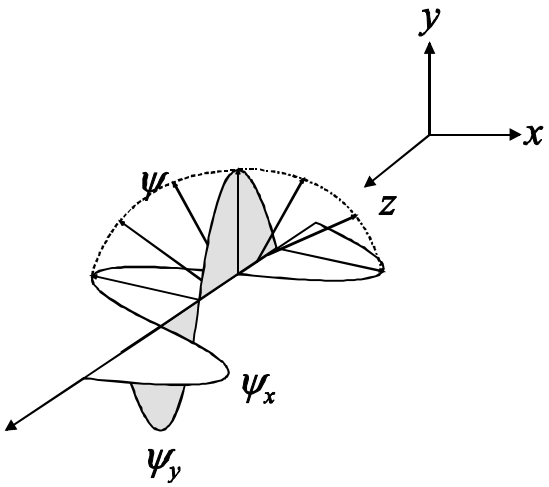

Figure 1.5 : *Left circularly polarised (LCP) optical field.*

It is evident from eq. (1.3) that linearly polarised light can be formed by combinations of RCP and LCP components. Adding or subtracting equal amplitude RCP and LCP components results in linear, horizontally and vertically polarised light respectively. Adding or subtracting equal amplitude RCP and LCP components with an arbitrary phase difference, $\pm f$, yields linear polarisation but orientated at an angle $\pm f/2$ to the *x*-axis.

Elliptical polarisation

As already discussed, eq. (1.1) represents the general case of elliptically polarised light. Rearranging eq. (1.1) gives

$$\left(\frac{y_y}{y_{oy}}\right)^2 + \left(\frac{y_x}{y_{ox}}\right)^2 - 2\left(\frac{y_y}{y_{oy}}\right)\left(\frac{y_x}{y_{ox}}\right)\cos f = \sin^2 f \qquad (1.4)$$

where f is the phase difference between the orthogonal components, i.e. $f = (f_x - f_y)$. Equation (1.4) represents an ellipse whose major axis lies at an angle q with the x - axis, where q is given by

$$\tan(2q) = \frac{2y_{ox}y_{oy}}{y_{ox}^2 + y_{oy}^2}\cos f \quad . \tag{1.5}$$

Again, an elliptically polarised optical field can be formed using RCP and LCP combinations of differing magnitude and phase.

1.2.2 Phenomenological description of the magneto-optic effects

The polar and longitudinal Kerr effects are the most commonly used in imaging applications. A simple phenomenological description of their 'origins' is discussed below.

In magnetic materials the RCP and LCP components of a polarised field display different refractive indices, $n^{\pm}$, and their Fresnel amplitude reflection coefficients, r^{+} and r^{-} respectively, will be different [23], such that

$$r^{\pm} = \frac{n^{\pm} - 1}{n^{\pm} + 1} = \left|r^{\pm}\right| \exp\{jf^{\pm}\} \tag{1.6}$$

and

$$\frac{r^{+}}{r^{-}} = \frac{\left|r^{+}\right|}{\left|r^{-}\right|} \exp\left\{j\left(f^{+} - f^{-}\right)\right\} \tag{1.7}$$

where the incident medium is free space. If the incident light is linearly polarised, i.e. the RCP and LCP components are of equal magnitude, then two limiting cases are defined. Firstly, when $\left|r^{+}\right| = \left|r^{-}\right|$ and $\left|f^{+}\right| \neq \left|f^{-}\right|$ which results in magnetic circular birefringence (MCB), where the reflected field is also linearly polarised but rotated by an amount $q_k = \left(f^{+} - f^{-}\right)/2$. The second case is when $\left|r^{+}\right| \neq \left|r^{-}\right|$ and $\left|f^{+}\right| = \left|f^{-}\right|$ which results in magnetic circular dichroism (MCD), where the reflected field is elliptically polarised, with the major axis aligned with the incident polarisation. However, in general the reflected field is determined by both MCB and MCD effects.

Thus, the reflected field is elliptically polarised with its major axis aligned at an angle q_k to the incident polarisation.

It is often convenient to represent the reflected light by Cartesian reflection coefficients, r_x and r_y. Hence, the reflected field is comprised of a component which is polarised in the same direction as the incident polarisation, the magnitude and phase of which is determined by r_x, and a magneto-optically induced component, the magnitude and phase of which is determined by r_y [24]. It is simple to switch between the two representations of the reflection coefficients, using the relationships

$$r_x = \frac{r^+ + r^-}{2} \quad , \quad r_y = j\frac{r^+ - r^-}{2} \tag{1.8}$$

If the incident illumination is linearly polarised along the x - axis, then upon reflection from the magnetic sample the light will be elliptically polarised, as illustrated in Fig. 1.6.

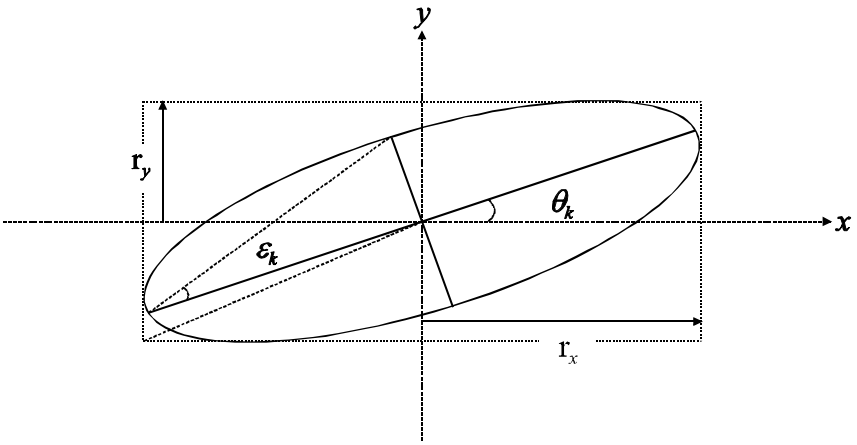

Figure 1.6 : *Elliptically polarised light, generated upon reflection from an MO surface.*

The magneto-optically induced Kerr signal illustrated in Fig. 1.6 can be described using the relations

$$\begin{aligned} \tan(2q_k) &= \tan(2a)\cos(f) = 2\frac{|r_x||r_y|}{|r_x|^2 - |r_y|^2}\cos(f) \\ \tan(a) &= \frac{|r_y|}{|r_x|} \quad , \quad \sin(2e_k) = \sin(2a)\sin(f) \end{aligned} \tag{1.9}$$

where q_k is the Kerr rotation angle, f is the phase difference between the orthogonal reflected components and e_k is the Kerr ellipticity, the tangent of which is defined as

ellipticity (ratio of major to minor axis). The Kerr signal is maximised, and ellipticity is removed, when the phase difference between the orthogonal components is zero, such that the plane of polarisation is merely rotated upon interaction with the sample. Since the Kerr rotation is characteristically small, around 0.2° to 0.4° for rare earth-transition metal (RE-TM) media [25], it is common to express the magneto-optically induced signal using small angles, i.e.

$$\left.\begin{aligned} q_k &= a\cos(f) \\ e_k &= a\sin(f) \end{aligned}\right\} f \neq 0 \qquad \left.\begin{aligned} q_k &= a \\ e_k &= 0 \end{aligned}\right\} f = 0 \quad . \tag{1.10}$$

The Kerr rotation, q_k, is proportional to the net magnetisation of the magnetic sample.

The small rotation of the plane of polarisation introduced by the magneto-optic effect can be measured using a variety of detection techniques [19,20,21,26,27,28,29,30,31]. The two most common MO detection strategies, the single detector MO configuration and the differential detector MO configuration, will be described in detail in Chapter 4.

1.3 Optical storage systems and the resolution limit

In optical storage systems a high information storage density is achieved using an optical arrangement similar to that of the scanning optical microscope [7,32,33,34]. The resolution of the scanning microscope is determined primarily by the diffraction limit of the optical system and the form of the incident illumination. The practical resolution limit is usually defined as the minimum distance separating two point objects at which they can just be resolved. Two criteria have been proposed to measure the so called two point resolution of an optical imaging system : the Rayleigh criterion and the Sparrow criterion. The Rayleigh criterion states that two point sources are resolvable when the maximum of the illuminance produced by the first point source falls on the first minima of the illuminance produced by the second point source. This is often expressed as the separation where the intensity at the midpoint

between the two point sources is 0.735 times the maximum intensity, and can be expressed as

$$resolution_{Rayleigh} \approx 0.6\frac{l}{NA} \tag{1.11}$$

where λ is the wavelength of illumination and NA is the numerical aperture of the lens. As such the Rayleigh criterion is a arbitrary limit. The sparrow criterion is concerned with the rate of change of the slope of the image at the midpoint [4,23,35,36,37].

1.4 The spatial frequency response of the scanning optical microscope

The spatial frequency response of an optical system is analogous to the temporal frequency response commonly used to characterise electrical systems. Spatial frequency is expressed in inverse metres (m^{-1}), or often in lines/mm. For example, a ruled grating with a line period p_g has a spatial frequency f_g given simply by

$$f_g = \frac{1}{p_g} \ . \tag{1.12}$$

A plane wave incident on such a grating will be split up into a strong zeroth-order plane wave and two weak first-order plane waves whose directions a_N are given by

$$\sin a_N - \sin a_o = \frac{Nl}{p_g} \qquad (N = -1,0,1) \tag{1.13}$$

where a_o is the angle of incidence and N is the order of the wave. Higher diffraction orders are present for low spatial frequencies of the grating. However, the contribution due to the higher diffraction orders is small compared to the zeroth and first orders and so are generally ignored [32,38]. The amplitude and phase variations of the diffracted orders depends primarily on the geometry of the grating and its position. Generally, as the period of the grating is reduced the amplitude of the diffracted order remains unchanged. However, the phase of the diffracted orders changes, and is given by

$$\Delta f_N = 2p\,\frac{Nu_o}{p_g} \tag{1.14}$$

where Δf_N is the phase of the diffracted order *N* and u_o is the displacement of the grating.

In the scanning microscope the detector is considered to be a unit circle, information regarding the grating position is determined by the area of overlap of the zeroth order and the first diffracted orders which falls within the detector area, as illustrated in Fig. 1.7.

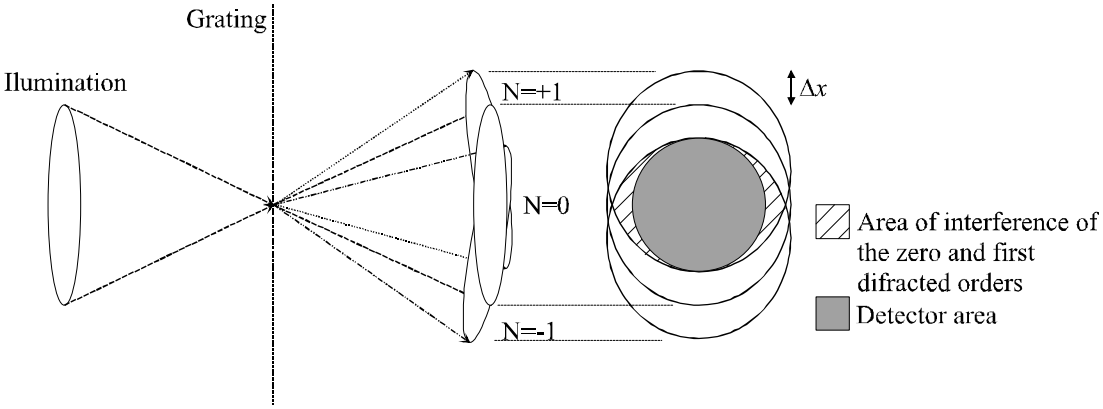

Figure 1.7 : *Area of overlap of the zero and first diffracted orders*

Δx represents the shift of the first diffracted order and is given by

$$\Delta x = \frac{l \diagup p_g}{NA} = \frac{l f_g}{NA} \qquad (1.15)$$

where *NA* is the numerical aperture of the objective lens.

Hence, it can be seen that at low frequencies, where the angle of diffraction of the first diffracted orders is small, a large proportion of overlap will occur between the zeroth and first diffracted orders and the resulting signal from the detector will be high. However, at higher spatial frequencies, where the angle of diffraction of the first diffracted orders is large, the overlap will be significantly reduced and so the resulting signal from the detector will be reduced also. The point at which the frequency will not be measured is given by the displacement of the first diffracted orders equal to the radius of the objective aperture. At this point the diffracted orders no longer overlap and this corresponds to the maximum observable spatial frequency and is given by the inverse of eq. (1.11), i.e.

$$f_{\max} = 2\frac{NA}{l} \quad . \qquad (1.15)$$

1.5 Summary and Objectives

This chapter has presented a brief review of the scanning optical microscope. The different optical configurations and their properties have been briefly discussed. The interaction between light and a magnetic surface, the magneto-optic effect, has been presented, illustrating how a scanning microscope can be developed which is sensitive to magneto-optic contrast. The frequency response of the scanning microscope, with reference to the diffraction grating, has been introduced. The remainder of this thesis concentrates on the development of a mathematical model that describes, in detail, the signal generation process in the scanning microscope, which employs a coherent, monochromatic, source, such as a laser.

In chapter 2 scalar diffraction theory and Fourier imaging will be presented. An expression is developed that describes the far-field diffraction pattern and this is seen to be similar to that expression representing the Fourier transform. Diffraction due to finite apertures and the thin lens will also be introduced.

Chapter 3 concentrates on the development of a mathematical framework describing the signal generated in the ordinary reflectance (non magneto-optic) scanning microscope. This is then be applied to imaging in the coherent, incoherent and Type 1 optical systems. A transfer function representation is developed that describes the signal generated by the Type 1 reflectance scanning microscope in a form where the properties of the optical channel are distinct from the properties of the sample. The partially coherent transfer function and the medium function will be introduced. A similar analysis will be applied for representing the signal generated in the Type 2, or confocal, reflectance scanning microscope.

In chapter 4 the single detector and differential detector magneto-optic scanning microscopes are illustrated. Expressions representing the signal generated in the magneto-optic scanning microscopes are developed, for both the Type 1 and confocal configurations, using an extension of the analysis developed in chapter 3.

In chapter 5 a computational method, the direct calculation approach, for modelling the signal generated in the Type 1 reflectance, single detector MO and differential detector MO scanning microscopes is presented. The direct calculation approach is shown to be particularly beneficial for generating theoretical two-dimensional images of objects.

In chapter 6 the computational implementation of the transfer function approach is presented for generating the theoretical one-dimensional response from all the scanning microscope configurations discussed. In particular the effects of pinhole size in the confocal configurations and analyser and wave-plate misalignment in the magneto-optic configurations on the readout signal will be presented.

Chapter 7 illustrates how the computational models may be used to investigate the signal generation process in optical storage systems. In particular the signal generation process in the CD-ROM, phase-change and magneto-optic storage systems, as well as future generation optical storage systems, such as digital versatile disk (DVD) is analysed.

Chapter 8 illustrates how the effects of common forms of aberrations observed in optical storage systems may be incorporated into the computational models. The effects of defocus, spherical aberration and astigmatism (as a result of substrate birefringence) are discussed.

In chapter 9 experimental results are presented to verify important theoretical results obtained in the previous chapters.